MnGe magnetic nanocolumns and nanowells

2010 Nanotechnology 21 255602

(http://iopscience.iop.org/0957-4484/21/25/255602)

Nanotechnology **21** (2010) 255602 (5pp) doi:10.1088/0957-4484/21/25/255602

MnGe magnetic nanocolumns and nanowells

Faxian Xiu[1], Yong Wang[2], Kin Wong[1], Yi Zhou[1], Xufeng Kou[1], Jin Zou[2,3] and Kang L Wang[1]

[1] Electrical Engineering Department, University of California at Los Angeles, CA 90095, USA
[2] Materials Engineering, The University of Queensland, Brisbane QLD 4072, Australia
[3] Centre for Microscopy and Microanalysis, The University of Queensland, Brisbane QLD 4072, Australia

E-mail: xiu@ee.ucla.edu

Received 25 March 2010, in final form 8 May 2010
Published 28 May 2010
Online at stacks.iop.org/Nano/21/255602

Abstract

We report a 'superlattice' growth method to produce well-aligned magnetic MnGe nanocolumns and nanowells by using low-temperature molecular-beam epitaxy. Both structural and magnetic properties show strong evidence of Mn_5Ge_3 precipitates and lattice-coherent nanostructures with different blocking temperatures. Magnetotransport measurements reveal positive and negative magnetoresistances for the nanowells and nanocolumns, respectively. This distinction can be explained by different spin scattering mechanisms under magnetic fields. Our results suggest a new growth strategy to achieve reproducible MnGe nanostructures, which facilitates the development of Ge-based spintronics and magnetoelectronics devices.

(Some figures in this article are in colour only in the electronic version)

1. Introduction

Since the discovery of ferromagnetic order in MnGe magnetic semiconductors, incorporating the spin degree of freedom into conventional Ge-based semiconductor devices has been under extensive study [1, 2]. The availability of spin polarized carriers in a semiconductor may open new strategies for data processing and complement conventional charge based micro- and nanoelectronics [3, 4]. This advantage stimulates tremendous efforts in developing MnGe dilute magnetic semiconductors (DMSs) [2]. To date, much progress has been made to address the fundamental challenges in Mn doping and improve film quality [1, 5–20]. Unfortunately, the low solubility of Mn in Ge remains a key obstacle to further improving the Curie temperature (T_c). Experimental data show that Mn has a strong tendency to aggregate to form metallic precipitates and nanostructures [7]. For example, under high-temperature growth conditions, metallic precipitates, such as Mn_5Ge_3 [11, 18] and $Mn_{11}Ge_8$ [17], are developed and are responsible for the room-temperature ferromagnetism. In contrast, with low-temperature growth, lattice-coherent MnGe nanostructures with irregular shapes are often observed, most likely originating from spinodal decomposition [13], similar to those of (Ga, Mn)N and (Zn, Cr)Te [13, 21].

While continuous efforts attempt to address the fundamental limitation of the Mn incorporation, the lattice-coherent nanostructures may facilitate spin injections into a traditional semiconductor because of less interface scattering and a small conductivity mismatch [22, 23]. In essence, a hybrid structure with a layer of a semiconductor and a ferromagnetic compound is needed to achieve spin injection. A precise control of the MnGe nanostructures may also enable the fabrication of nanodevices such as nanodot memories and nanochannels for spin injection. However, creating such hybrid systems is rather challenging, particularly considering the random nucleation of the MnGe nanostructures. Jamet *et al* [7] recently employed a eutectoid growth method to fabricate self-organized MnGe nanocolumns. Other groups also tried various growth conditions to control the MnGe nanostructures by low-temperature molecular-beam epitaxy (MBE) [10, 11]. However, up to now, the controllability of these nanostructures still remains difficult and elusive. In this paper, we report a 'superlattice' approach by alternately growing MnGe and Ge layers with designated thicknesses. Well-controlled MnGe nanostructures can be obtained with excellent reproducibility when the growth temperature and thicknesses of MnGe and Ge are properly designed. Since the MnGe nanostructures are embedded in the Ge matrix, this material system combines

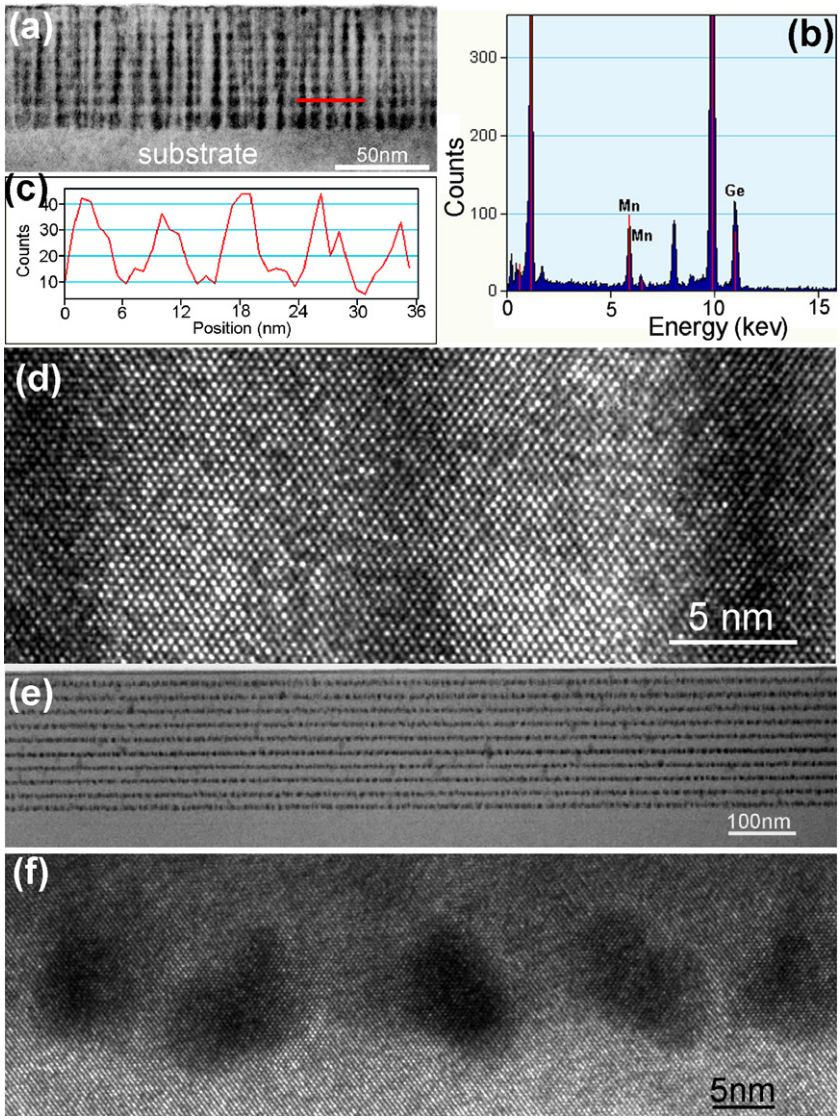

Figure 1. Structural properties of the MnGe nanocolumns and nanowells. (a) A typical cross-sectional TEM image of nanocolumns; (b) EDS composition analysis taken from a MnGe nanocolumn, which shows Mn and Ge peaks; (c) an EDS line scan of Mn in the STEM mode, revealing the Mn distribution; (d) a high resolution TEM image of MnGe nanocolumns; (e) a typical TEM image of MnGe nanowells; (f) a high resolution TEM image of a single MnGe nanowell consisting of MnGe nanodots.

both the magnetic properties from the MnGe nanostructures and important semiconductor characteristics, providing an extraordinary material candidate for future spin electronics devices.

2. Experimental details

The 'superlattice' growth approach was carried out by alternating the growth of Mn-doped Ge and undoped Ge thin layers with a solid source MBE. High-purity Ge (99.9999%) and Mn (99.99%) sources were evaporated by conventional high-temperature effusion cells. During the growth, a Ge growth rate of 0.2 Å s^{-1} with an adjustable Mn flux as the dopant source was used. A high-quality single-crystalline Ge buffer layer was first deposited at 250 °C with a thickness of about 50 nm. The growth temperature was then decreased to 70 °C for the subsequent 'superlattice' growth. Note that 70 °C was found to be the optimized growth temperature for the fabrication of the reproducible nanostructures. Ten periods of Ge and MnGe layers were grown for each case. By adjusting the nominal thicknesses of the Ge spacer layer from 6 to 25 nm while keeping the MnGe layer at about 4 nm, MnGe nanocolumns and nanowells were obtained, respectively. More than 90% of films in 50 runs exhibit the nanocolumn and nanowell structures, showing good reproducibility. All films were grown on semi-insulating GaAs substrates to avoid the substrate conducting effect. After growth, the structural and magnetic properties were conducted by transmission electron microscopy (TEM), energy dispersive spectroscopy (EDS), a superconducting quantum interference device (SQUID) and a physical property measurement system (PPMS).

3. Results and discussion

Figure 1(a) is a typical cross-sectional TEM image of the MnGe nanocolumns. From this figure, well-aligned

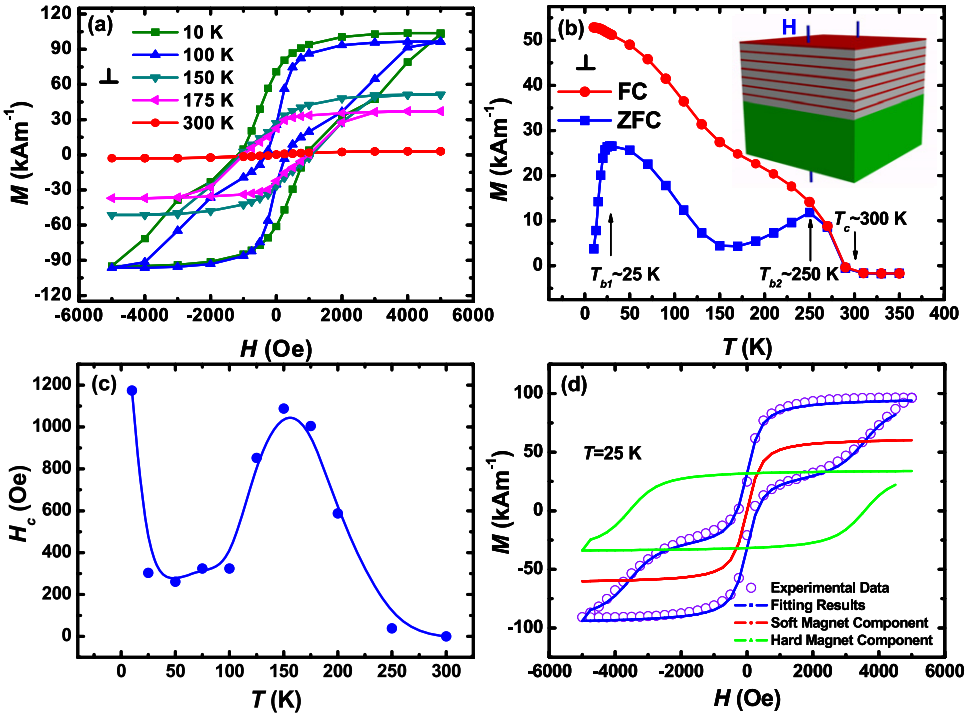

Figure 2. Magnetic properties of the MnGe nanowells. (a) Temperature dependent hysteresis loops with the sample surface perpendicular to the external magnetic field. (b) ZFC and FC curves. Inset is a schematic drawing of the sample setup during the SQUID measurements. (c) Coercivity as a function of temperature. (d) A hysteresis loop at 25 K. The hysteresis loop is the sum of two magnetic components, a hard component (Mn_5Ge_3) and a soft one.

nanocolumns with dark contrast can be clearly observed. The composition of the dark nanocolumns was analyzed by the EDS experiments in the scanning TEM (STEM) mode and the result is shown in figure 1(b). It should be noted that the EDS result taken locally from one nanocolumn as the beam probes can be down to 1 nm in the STEM mode. The Mn and Ge peaks are clearly seen and the Mn concentration is determined to be up to 19%. Figure 1(c) is the EDS line scan of Mn, which clearly shows the Mn distribution and the size of the MnGe nanocolumns. To reveal the detailed lattice structure of the nanocolumns, high resolution TEM (HRTEM) experiments were carried out and the result is shown in figure 1(d). Careful examination of the HRTEM image verifies that the MnGe nanocolumns have the same diamond structure as that of the Ge matrix, showing a coherent growth. A similar phenomenon was previously reported in MnGe nanocolumns [7] and nanodots [9]. Figure 1(e) shows a typical TEM image of MnGe nanowells with ten periods. Noticeably, the nanowell is composed of dense MnGe nanodots, as shown in figure 1(f). Like the nanocolumn case, the MnGe nanodots inside the nanowells are also coherent with the surrounding Ge matrix. The diameter of these nanostructures has a typical range of 4–10 nm; and the Mn concentration can be tuned from 11% up to 19% in different samples, depending upon the nominal Mn concentration.

It should be noted that, other than the coherent MnGe nanostructures, some metallic precipitates can occasionally be found in our films. These precipitates are most likely attributed to the formation of the Mn_5Ge_3 phase [11]. The SQUID measurements, however, are much more sensitive to the presence of Mn_5Ge_3 clusters even at very low concentration [13]. Indeed, our magnetic measurements show strong evidence of both the Mn_5Ge_3 precipitates and the lattice-coherent Mn-rich nanostructures, which are responsible for the ferromagnetic properties in different temperature regions. These observations are in excellent agreement with Devillers *et al* [13] and Ahlers *et al* [18]. Due to the similarity of the magnetic properties, we take the case of the MnGe nanowells as an example. The film exhibits a saturation moment of 104 kA m^{-1} (figure 2(a) at 10 K) compared with the reported value of 120 kA m^{-1} for $MnGe_2$ nanocolumns [7]. The magnetic moments per Mn atom can be estimated to be 0.24 μ_B. Provided that each Mn has a theoretical moment of 3 μ_B [1, 24], this gives a fraction of roughly 8% of Mn being activated in the MnGe layer.

Zero-field cooled magnetization (ZFC) experiments were performed by cooling the sample under zero magnetic field from 350 to 10 K, and subsequently measuring the magnetic moments while the sample was warmed up under a field of 200 Oe. For the field cooled magnetization (FC) process, however, the sample is cooled through its Curie temperature in the presence of a magnetic field (200 Oe). The difference between these two processes gives an insight into phase transformation, the blocking temperature (T_b), and the Curie temperature. As shown in figure 2(b), the MnGe nanowells display a substantial difference between the ZFC and FC curves, which is interpreted by blocking transitions of superparamagnetic particles [13], i.e., T_{b1} is associated with the lattice-coherent nanostructures and T_{b2} corresponds to the Mn_5Ge_3 precipitates. The anisotropy energy E_A can be

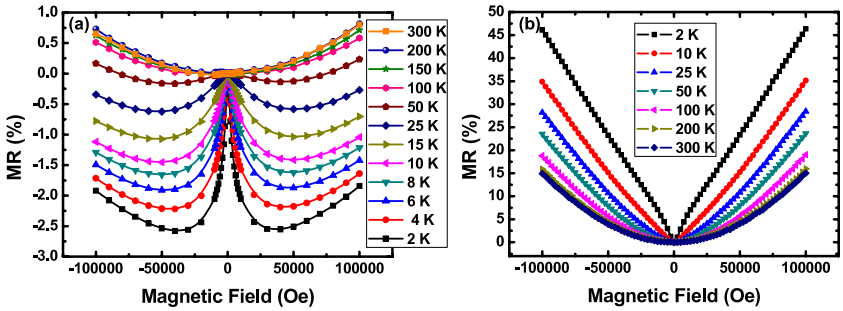

Figure 3. Magnetotransport measurements for the MnGe nanocolumns and the nanowells in (a) and (b), respectively. The MnGe nanocolumns show negative MR below 50 K while a positive component becomes evident at high temperatures. For the MnGe nanowells, however, positive MR was observed in the whole temperature range from 2 to 300 K.

described by $E_A = KV\sin^2(\theta)$, where K is the anisotropy energy density, V the particle volume, and θ the angle between the magnetic moment and anisotropy axis [25]. In the temperature regime of 250 K $< T <$ 300 K, the system falls into a superparamagnetic regime. The magnetization direction can randomly flip during the time of the measurement due to thermal activation. If the temperature decreases below 250 K, however, the energy barrier (E_A) can block the magnetic moments in a direction either parallel or antiparallel to the easy axis [18]. Likewise, at a lower transition temperature of $T_{b1} = 25$ K, the lattice-coherent MnGe nanostructures would undergo a similar superparamagnetic transition, but with much lower blocking temperature because of a smaller volume (V) compared with Mn_5Ge_3 clusters [25].

The hysteresis loops in the temperature range between 25 and 100 K present a low-field narrowing (figures 2(a) and (d)). This is verified by anomalous behavior of the coercive field as a function of temperature, as shown in figure 2(c). The experimental coercive field decreases with temperature up to 50 K; but increases in the range of 50–150 K from 261 to 1088 Oe. For higher temperatures, coercivity decreases as temperature increases, until it completely disappears around 300 K. The distorted shape of the hysteresis loops in the intermediate range of temperatures and the anomalous temperature dependence of the coercive field suggest that the magnetic response in the MnGe sample is indeed due to two phase contributions [26]. As already pointed out, there are two types of clusters in the MnGe films, i.e., the Mn_5Ge_3 precipitates and the lattice-coherent nanostructures. Accordingly, we can fit the hysteresis loops as the sum of two magnetic components [26], a hard component (Mn_5Ge_3), and a soft one with a paramagnetic behavior in which the coercive field is set to zero (at 25 K). Each component is fitted with a Langevin function [27],

$$M(H) = \sum_{i=1,2} M_s^i L[C^i(H \pm H_c^i)], \qquad (1)$$

where L is the Langevin function, M_s is the saturation magnetization, H_c is the coercivity, C is a proportionality constant and the superscript $i = 1, 2$ refers to the hard and the soft component respectively (see figure 2(d)).

Since the overall MnGe nanostructures are ferromagnetic, with a T_c of about 300 K, it is of great interest to study their magnetotransport properties. The samples were fabricated into standard Hall bars with a typical channel width of 500 μm. For all measurements, the external magnetic field (H) was applied perpendicular to the sample surface while the measurement current is in-plane. The magnetoresistance (MR) measurements were performed from 2 to 300 K with an external magnetic field up to 10 T. For MnGe nanocolumns, a negative MR was observed up to 50 K (figure 3(a)), which is in good agreement with the reported disordered MnGe nanostructures, where the MR is negative in the low-temperature region ($T <$ 20 K). The origin of negative MR has been explained by a spin scattering mechanism [19]. The carrier transport between the nanocolumns or disordered nanoclusters with an appropriate spin alignment is believed to result in spin-dependent scattering. Higher magnetic fields would align the magnetic domains in the nanocolumns preferentially in the out-of-plane direction, leading to the reduction of spin scattering in the carrier transport direction (in-plane).

The MnGe nanowells, however, present a positive MR in the entire temperature range (figure 3(b)). Traditionally, the positive MR is attributed to the Lorentz force in the semiconductor matrix, which deflects the carriers during the transport process [28]. The resulting MR is positive and proportional to $(\mu H)^2$ under low magnetic fields [7] ($H \leqslant 1$ T in our case) where μ is the semiconductor mobility (units $m^2\ V^{-1}\ S^{-1}$ or T^{-1}) and H is the magnetic field. However, with a simple calculation, the estimated orbital MR is too small to explain the relatively large MR observed from the nanowell sample. Instead, besides the effect of orbital MR, the high-density magnetic nanodots in the nanowells could contribute to the MR ratios due to an enhanced geometric MR effect, from which the current path could be significantly deflected when large magnetic fields were applied to the magnetic nanostructures [7, 28–30]. To elucidate the underlying physics of the geometrical effect, we consider the current density and the total electric field in semiconductors, which can be described by $j = \bar{\sigma} E$, where the magneto-conductivity tensor is given by [30, 31],

$$\bar{\sigma}(H) = \begin{pmatrix} \frac{\sigma}{1+\beta^2} & \frac{\sigma\beta^2}{1+\beta^2} & 0 \\ \frac{-\sigma\beta^2}{1+\beta^2} & \frac{\sigma}{1+\beta^2} & 0 \\ 0 & 0 & \sigma \end{pmatrix}. \qquad (2)$$

Here, $\beta = \mu H$. At zero magnetic field, β vanishes. The conductivity tensor is diagonal when there is no magnetic field; and the current density can be simply described by $j = \sigma E$. Under this scenario, the current flowing through the material is concentrated in the metallic region, which behaves like a 'short circuit' [7, 30, 31]. However, at high magnetic fields ($\beta \gg 1$), the off-diagonal terms of $\bar{\sigma}(H)$ dominate ($j \perp E$), and the current becomes tangent to the nanodots. The current is deflected to flow around the metallic clusters, resembling an 'open circuit' state. The transition from the 'short circuit' at the zero field to the 'open circuit' at high fields produces an increase of resistance, i.e., a positive geometrically-enhanced MR [30, 31]. The above explanation has been successfully applied to several material systems, including Au/InSb [29] and MnAs/MnGaAs [30]. Similarly, the geometrically-enhanced MR was identified in $MnGe_2$ nanostructures with a high Mn concentration of ~33% [7].

While the geometrical effect offers a good explanation for the positive MR (figure 3(b)), the reduced spin scattering would generate a negative MR, as observed in the nanocolumn case (figure 3(a)). Therefore, we anticipate that more than one mechanism may be relevant to MR at low temperatures. The final results could depend on the competition between different mechanisms [30]. The magnetotransport properties of the MnGe nanocolumns and nanowells suggest that, by manipulating the film structures, different MRs can be engineered. This property offers a great advantage for designing spintronics devices in which the direction of spin injection relative to the magnetic domain is critical.

4. Conclusions

In conclusion, we have fabricated MnGe nanocolumns and nanowells with a Curie temperature of ~300 K by low-temperature MBE. The magnetic property measurements revealed the presence of two phases in both nanocolumns and nanowells: the lattice-coherent nanostructures ($T_{b1} \sim$ 25 K) and the Mn_5Ge_3 metallic precipitates ($T_{b2} \sim$ 250 K). The MR measurements showed different magnetotransport mechanisms, involving both geometrical and spin scattering effects. The understanding and fabrication of MnGe nanostructures via the 'superlattice' approach provides an important platform for the design of future spintronics and magnetoelectronics devices.

Acknowledgments

The Focus Center Research Program-Center on Functional Engineered Nano Architectonics, Western Institution of Nanoelectronics, Intel (Spin-Gain FET project) (UCLA) and the Australia Research Council (University of Queensland, Australia), are acknowledged for their financial supports of this project.

References

[1] Park Y D, Hanbicki A T, Erwin S C, Hellberg C S, Sullivan J M, Mattson J E, Ambrose T F, Wilson A, Spanos G and Jonker B T 2002 *Science* **295** 651–4
[2] Xiu F, Wang Y, Kim J, Hong A, Tang J, Jacob A P, Zou J and Wang K L 2010 *Nat. Mater.* **9** 337–44
[3] Prinz G A 1998 *Science* **282** 1660–3
[4] Song J H, Lee J J, Cui Y, Ketterson J B and Cho S 2005 *J. Magn. Magn. Mater.* **286** 41–5
[5] Li A P, Wendelken J F, Shen J, Feldman L C, Thompson J R and Weitering H H 2005 *Phys. Rev.* B **72** 195205
[6] van der Meulen M I, Petkov N, Morris M A, Kazakova O, Han X, Wang K L, Jacob A P and Holmes J D 2008 *Nano Lett.* **9** 50–6
[7] Jamet M *et al* 2006 *Nat. Mater.* **5** 653–9
[8] Bihler C, Jaeger C, Vallaitis T, Gjukic M, Brandt M S, Pippel E, Woltersdorf J and Gosele U 2006 *Appl. Phys. Lett.* **88** 112506
[9] Bougeard D, Ahlers S, Trampert A, Sircar N and Abstreiter G 2006 *Phys. Rev. Lett.* **97** 237202
[10] Li A P *et al* 2007 *Phys. Rev.* B **75** 201201
[11] Wang Y, Zou J, Zhao Z, Han X, Zhou X and Wang K L 2008 *Appl. Phys. Lett.* **92** 101913
[12] De Padova P *et al* 2007 *Surf. Sci.* **601** 2628–31
[13] Devillers T, Jamet M, Barski A, Poydenot V, Bayle-Guillemaud P, Bellet-Amalric E, Cherifi S and Cibert J 2007 *Phys. Rev.* B **76** 205306
[14] Ahlers S, Bougeard D, Sircar N, Abstreiter G, Trampert A, Opel M and Gross R 2006 *Phys. Rev.* B **74** 214411
[15] Tsui F, Collins B A, He L, Mellnik A, Zhong Y, Vogt S and Chu Y S 2007 *Appl. Surf. Sci.* **254** 709–13
[16] Jaeger C, Bihler C, Vallaitis T, Goennenwein S T B, Opel M, Gross R and Brandt M S 2006 *Phys. Rev.* B **74** 045330
[17] Cho S, Choi S, Hong S C, Kim Y, Ketterson J B, Kim B-J, Kim Y C and Jung J-H 2002 *Phys. Rev.* B **66** 033303
[18] Ahlers S, Bougeard D, Riedl H, Abstreiter G, Trampert A, Kipferl W, Sperl M, Bergmaier A and Dollinger G 2006 *Physica* E **32** 422–5
[19] Park Y D, Wilson A, Hanbicki A T, Mattson J E, Ambrose T, Spanos G and Jonker B T 2001 *Appl. Phys. Lett.* **78** 2739–41
[20] Chen J, Wang K L and Galatsis K 2007 *Appl. Phys. Lett.* **90** 012501
[21] Fukushima T, Sato K, Katayama-Yoshida H and Dederichs P H 2006 *Japan. J. Appl. Phys.* 2 **45** L416–8
[22] Kioseoglou G, Hanbicki A T, Sullivan J M, van't Erve O M J, Li C H, Erwin S C, Mallory R, Yasar M, Petrou A and Jonker B T 2004 *Nat. Mater.* **3** 799–803
[23] Tanaka M 2002 *Semicond. Sci. Technol.* **17** 327–41
[24] Stroppa A, Picozzi S, Continenza A and Freeman A J 2003 *Phys. Rev.* B **68** 155203
[25] Jacobs I S and Bean C P 1963 *Magnetism* (New York: Academic)
[26] Verna A *et al* 2006 *Phys. Rev.* B **74** 085204
[27] Passacantando M, Ottaviano L, Grossi V, Verna A, D'Orazio F, Lucari F, Impellizzeri G and Priolo F 2007 *Nucl. Instrum. Methods Phys. Res.* B **257** 365–8
[28] Yuldashev S U, Shon Y, Kwon Y H, Fu D J, Kim D Y, Kim H J, Kang T W and Fan X 2001 *J. Appl. Phys.* **90** 3004–6
[29] Solin S A, Thio T, Hines D R and Heremans J J 2000 *Science* **289** 1530–2
[30] Heimbrodt W, Klar P J, Ye S, Lampalzer M, Michel C, Baranovskii S D, Thomas P and Stolz W 2005 *J. Supercon.* **18** 315–20
[31] Schlovskii B I and Lfros E A 1984 *Electronics Properties of Doped Semiconductors* (Berlin: Spinger)